DE GRUYTER Adv. Opt. Techn. 2014; 3(4): 407–416

Research Article

Abraham Mario Tapilouw, Liang-Chia Chen*, Nguyen Xuan-Loc and Jin-Liang Chen

Multi-function optical characterization and inspection of MEMS components using stroboscopic coherence scanning interferometry

Abstract: A Micro-electro-mechanical-system (MEMS) is a widely used component in many industries, including energy, biotechnology, medical, communications, and automotive industries. However, effective inspection systems are also needed to ensure the functional reliability of MEMS. This study developed a stroboscopic coherence scanning Interferometry (SCSI) technique for measuring key characteristics typically used as criteria in MEMS inspections. Surface profiles of MEMS both static and dynamic conditions were measured by means of coherence scanning Interferometry (CSI). Resonant frequencies of vibrating MEMS were measured by deformation of interferogram fringes for out-of-plane vibration and by image correlation for in-plane vibration. The measurement bandwidth of the developed system can be tuned up to three megahertz or higher for both in-plane and out-of-plane measurement of MEMS.

Keywords: dynamic profile measurement; MEMS; resonant frequency detection; white light interferometry.

DOI 10.1515/aot-2014-0031
Received April 18, 2014; accepted June 30, 2014

1 Introduction

In Micro-Electro-Mechanical-Systems (MEMS), mechanical elements, sensors, actuators, and electronics are integrated by using VLSI processing techniques [1, 2]. The mechanical and chemical processes during MEMS fabrication affect the final shape and characteristics of the MEMS. Undesired defects can substantially affect the performance of the MEMS during its operation in dynamic modes, in which vibration is either in-plane or out-of-plane. Thus, static and dynamic characteristics of MEMS must be accurately measured during inspection. Static characteristics, which include dimensions and surface topography, can be measured by common phase-shifting interferometry (PSI) or by coherence scanning interferometry (CSI) systems.

Dynamic characteristics of MEMS can be categorized as either in-plane vibration or out-of-plane vibration. Many methods used to measure dynamic out-of-plane vibratory modes of micromechanical devices use single-beam laser Doppler vibrometers [3]. However, these techniques are only effective for slow point-type scanning measurement and are very time consuming. Laser phase-shifting interferometry can also be combined with stroboscopic lighting [4–6] to measure the surface of a vibrating MEMS. The surface measured or reconstructed in the study is referred as an areal surface due to a limited detection field of view in microscopic imaging. Digital holographic microscopy (DHM), which can be used to measure surface topography by using a holographic image, has also been applied in MEMS measurement by using a laser source and high speed camera for hologram acquisition [7].The technique enables measurement of mechanical behavior in MEMS. However, a drawback of the holographic microscopic is noisy fringe patterns caused by laser speckle phenomenon [8], which require further image processing techniques to reconstruct the surface topography. Another limitation of using single wavelength for measurement is that the measurable step-height detection range is limited by a quarter of wavelength. To address this limitation, Nakano et al., [9] used a pulsed laser diode to overcome this issue, Nakano et al., [9] used a pulsed laser diode for stroboscopic phase-shifting interferometry.

***Corresponding author: Liang-Chia Chen,** Department of Mechanical Engineering, National Taiwan University, e-mail: lchen@ntu.edu.tw
Abraham Mario Tapilouw: Center for Measurement Standards, Industrial Technology Research Institute, Taiwan
Nguyen Xuan-Loc and Jin-Liang Chen: R&D department, Allied Engineering & Consultant, Inc. (AEC), Taipei, Taiwan

www.degruyter.com/aot
© 2014 THOSS Media and De Gruyter

Many studies in the literature have performed detailed studies of SCSI. Measurement accuracy mainly depends on the duty cycle of the light source. De Groot [10] performed an approximate simulation study of the effect of pulse duty cycle on SCSI measurements. Pettitgrand and Bosseboeuf [11] have also used stroboscopic phase shifting interferometry for a comprehensive study of the effect of duty cycle on contrast degradation and errors in profile measurements. Chen et al. [12] developed a signal deconvolution technique for improving contrast in interferograms acquired at a long-pulse duty cycle and then theoretically and experimentally verified the effect of duty cycle on measurement errors. In all of the above studies, the aim was to improve dynamic measurement accuracy without having to upgrade the current instruments. A recent development in dynamic white light interferometry (WLI) measurement is employing a 4D microscope with a high speed camera and a FPGA for real-time image processing [13]. A continuing challenge in SCSI systems is developing an effective calibration method for validating the measurement accuracy. Seppä et al., [14] developed a traceable calibration artifact with a reproducible out-of-plane vibration. The developed artifact was calibrated with a laser interferometer, and the artifact was reproducible with an estimated standard uncertainty of 2.3 nm.

Most SCSI systems use phosphor-based LED lighting. Its limitations include interferogram ringing caused by non-Gaussian spectrum [15] and phosphorescence effects resulting in a switching time longer than that in single color LEDs [12]. Heikkinen et al., [16] developed a stroboscopic WLI system with a non-phosphor LED source. This technique is performed by modifying the light source with a non-phosphor white LED and used a cyan LED to remove the side peak of the interferogram commonly seen in WLI using LED as the light source. The shortest pulse that can be produced by the light source in this setup is 6.36 ns, and the system can measure a vibrating sample up to 2.72 MHz. In contrast, in-plane vibrations of MEMS can be made at nanometer resolution by using the correlation of synchronous images [17]. The above references reveal the main factors affecting the accuracy of dynamic measurements for both in-plane and out-of-plane vibration.

This study developed techniques and strategies for performing static and dynamic measurements of MEMS by using SCSI. Although various techniques regarding SCSI for dynamic characterization of MEMS has been developed for many years [12, 18–20], an SCSI optical testing platform has not been integrated with multi dynamic testing for MEMS characterization. Integrating these techniques enables the measurement of multiple MEMS characteristics with a single measurement platform. This article proposes an integrated system and describes its measurement principle and procedure. The proposed system can measure characteristics such as surface topography in both static and dynamic conditions by means of phase shifting interferometry and CSI, resonant frequency detection by means of white light interferometry for out-of-plane vibrating samples and image correlation for in-plane vibrating samples. Repeatability and accuracy are evaluated by comparing the measurement results with reference instruments and by measuring standard samples.

2 System design principle and its verification

Figure 1 illustrates the developed testing system, and Figure 1A, B show the principle of the testing system and the developed platform, respectively. The system employs replaceable microscopic objectives for achieving different optical magnification with a tunable field of view (FOV). The microscope is equipped with a motorized X-Y stage and a nanometer-scale piezo electric transducer for performing vertical scans and phase shifting interferometric measurements. Figure 1A is schematic diagram of the developed optical system. The diagram shows that a Michelson or Mirau interferometric objective is used for full-field stroboscopic interferometry measurement. The optical system uses a set of optical lenses to collimate incident light from the light source module, which produces a parallel white light beam that illuminates the measured surface and the reference mirror. A single superluminescent light-emitting diode (SLED) is driven in pulse mode for stroboscopic dynamic measurement or is driven in continuous wave mode for static surface profilometry. Stroboscopic source illumination and signal synchronization are used to capture shifted periodic images during dynamic measurement of a vibrating sample. The synchronization system comprising a central control unit, a synchronous control unit, a vibration-driving unit, a light-emitting unit and an image-acquiring unit, is specifically designed for consistent motion-free image detection. Images can be acquired synchronously by coupling the image-acquiring unit to the central control unit. Signal synchronization is accurate to within several nano seconds. A driver in the lens module controls the interference objective when performing scanning interferometric measurements in surface profilometry. The beamsplitter receives the strobed light, guides it into a Mirau interferometric objective, and then projects it onto the vibrating sample.

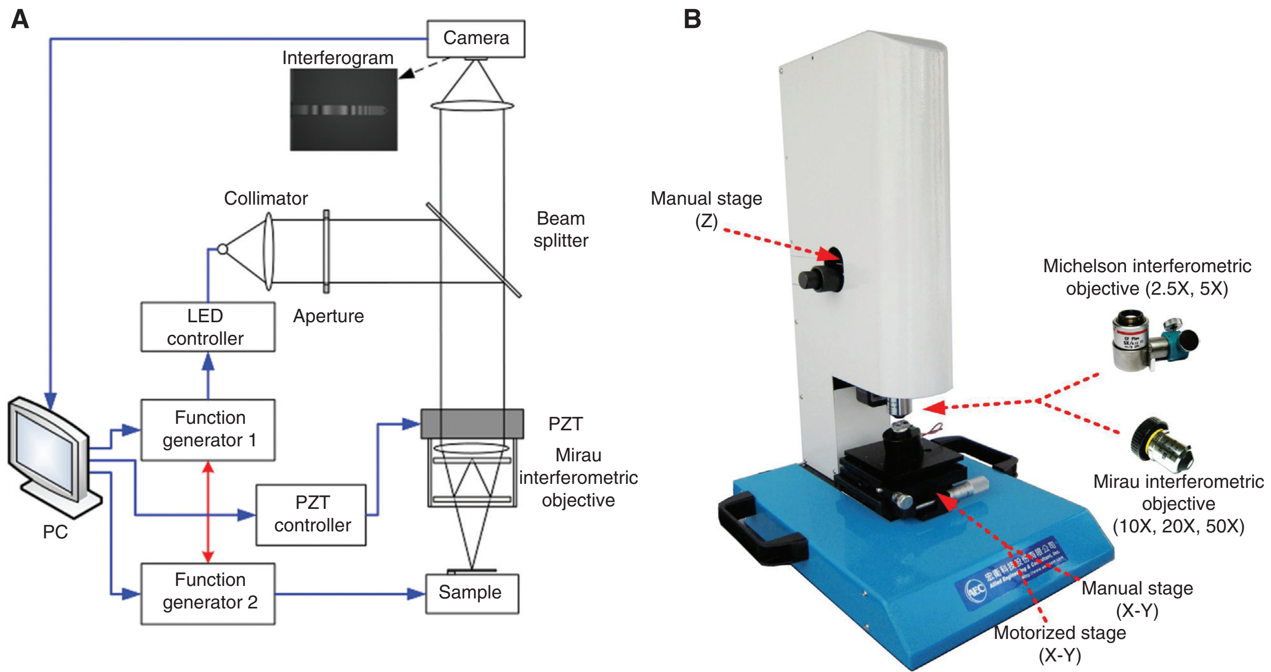

Figure 1 Developed SCSI system: (A) design of the testing system with stroboscopic lighting and (B) developed measurement platform.

For synchronization control, Figure 2A shows that the SLED pulsed light spectrum is generated and driven using a function generator while the function generator is synchronized with another function generator that produces an actuating sinusoidal signal for exciting the tested sample. Synchronizing these two function generators is essential for accurate measurement of either in-plane or out-of plane vibration. Figure 2B exhibits the sinusoidal signal for exciting the sample at the desired vibration and also shows the pulse signal used for stroboscopic lighting.

Shown in Figure 2B, the phase delay between the sample vibration and the pulse signal (θ) can be controlled to enable reconstruction of the vibration mode of the sample. The phase delay, θ_1, is applied to perform reconstruction of the object at 0° while the phase delay, θ_2, is employed to perform reconstruction of the object at 90°. Using a similar principle, the complete vibration mode of the object can be reconstructed by applying different phase delays between the pulse light and vibration signal in one period of 2π. Vibration mode reconstruction

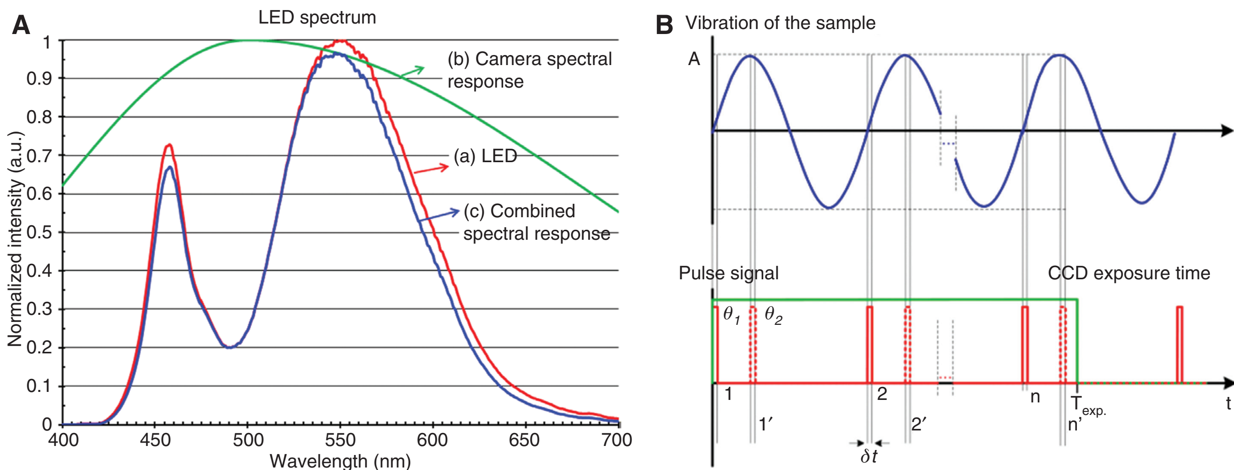

Figure 2 (A) Spectrum of the employed LED light source as measured by spectrometer; (B) synchronization signals between sinusoidal signal for vibrating sample and pulse signal for lighting.

can be performed either for in-plane vibration or out-of-plane vibration. Accuracy of the measurement is mainly determined by two factors, namely synchronization of the function generators and the duty cycle of the pulse signal.

2.1 Static and dynamic profile measurement

In the developed system, profile measurement is performed using CSI and PSI with an additional narrow bandpass filter to generate quasi-monochromatic light source. Static measurement accuracy is validated using standard calibration artifacts and varying step heights.

In CSI measurements, the intensity of the interferometric fringe in an arbitrary region of the object under test can be expressed as

$$I(z)=I_0+[I+C(z\text{-}z_0)\cos(k(z\text{-}z_0)+\phi_0)] \quad (1)$$

Where $I(z)$ is the interferometric light intensity that varies with position z of the test surface; I_0 is the mean interferometric light intensity; $C(z\text{-}z_0)$ is the interference contrast; $k=2\pi/\lambda$ is the wave number of the light source; z_0 is the position of zero optical difference; and ϕ_0 is the phase offset of the interferogram.

To measure a dynamic object vibrating at a certain frequency, Equation (1) can be rewritten as

$$I(z(\omega,t,\Lambda))=I_0[1+C(z(\omega,t,\Lambda))\cos(k(\omega,t,\Lambda))+\phi_0)] \quad (2)$$

Here $z(\omega, t, \Lambda)=z_0+\Lambda\sin(\omega t+\varphi)$ is the vibration displacement of the tested object as the function of time; Λ is the amplitude of the vibration; and ϕ_0 is the initial phase of the interferogram.

In SCSI, the light pulse can be modeled by a Gaussian function synchronized with the vibration signal as follows:

$$P(t)=P_c\cdot e^{-(t\text{-}t_c)^2/2\delta_t^2} \quad (3)$$

where δ_t is the standard deviation in the stroboscopic pulse, P_c is the maximum light intensity, and t_c is the center of the stroboscopic pulse.

Intensity of the light pulse can be expressed as a function of the height of the tested object (z) as follows:

$$P(z(\omega,t,\Lambda))=P_c\cdot e^{-\left(\frac{1}{v}(z(\omega,t,\Lambda)\text{-}z_c)\right)^2/2\delta_{z\tau}^2} \quad (4)$$

where z_c is the center position of the sample associated with the pulse center, $\delta_z\tau$ is the light intensity distribution along the z axis, and v is the vibrating speed of the object under test.

The interference light beam recorded by the camera, I_s, is modeled as the output of the convolution operation between the stroboscopic pulse $P(z(\omega, t))$ and the vibratory interferometric light intensity (I) of a vibratory object as follows [12]:

$$I_s(z(\omega,t,\Lambda))=I(z(\omega,t,\Lambda))*P(z(\omega,t)) \quad (5)$$

Therefore, the vibratory interferometric signal of SWLI can be modeled as

$$I_s(z(\omega,t,\Lambda),k)=\left[\int_{k_0}^{k_n} I_0[1+C(z(\omega,t,\Lambda))\cos(k(z(\omega,t,\Lambda))+\phi_0)]dk\right]*\left[P_c e^{-\left(\frac{1}{v}(z_e+z_1(\omega,t)\text{-}z_c)\right)^2/2\delta_{z\tau}^2}\right] \quad (6)$$

The pulse length (δt) of the light beam can be considered by rewriting Equation (6) as

$$I_s(z(\omega,t,\Lambda),k)=\int_{\theta_0}^{\theta_0+\delta t} I_s(z(\omega,t,\Lambda),k)*P(z(\omega,t))dt$$
$$I_s(z(\omega,t,\Lambda),k)=\int_{\theta_0}^{\theta_0+dt}\left\{\left[\int_{k_0}^{k_n} I_0[1+C(z(\omega,t,\Lambda))\cos(k(z(\omega,t,\Lambda))+\phi_0)]dk\right]*\left[P_c e^{-\left(\frac{1}{v}(z_e+z_1(\omega,t)-z_c)\right)^2/2\delta_{z\tau}^2}\right]\right\}dt \quad (7)$$

where θ_0 is the initial time of the stroboscopic pulse corresponding to the phase delay of the pulse with respect to the sinusoidal vibration and δt is the length of the stroboscopic pulse cycle time.

In PSI measurements, intensity of the interferometric fringe is calculated using an equation similar to Equation (1) but with $C(z)$ assumed to be a constant within the depth of field of the interference objective. For the five-step PSI, five interferograms are captured with a 90° phase shift (equivalent to $\lambda_c/8$), and the object phase is calculated using the following five-step phase wrapping algorithm:

$$\phi=\tan^{-1}\frac{2*(I_1\text{-}I_3)}{2I_2\text{-}I_4\text{-}I_0} \quad (8)$$

where ϕ is the phase of the surface, I_n is the intensity of the interferogram at certain phase step (n=0 for 0°, n=1 for 90°($\pi/2$), n=2 for 180°(π), n=3 for 270°($3\pi/2$), n=4 for 360°(2π)).

The resulting wrapped phase is first converted from 0°–180° into 0°–360° range by performing Euler transformation. Phase unwrapping is then performed to

reconstruct phase map of the test surface. Since the arctangent function produces results in the range (-π/2, π/2] and the phase value is actually in [0, 2π), the Euler Equation is required to map the phase into [0, 2π).

Suppose

$$\phi = \tan^{-1}\left(\frac{\sin\phi}{\cos\phi}\right) = \tan^{-1}\left(\frac{\mathrm{Im}}{\mathrm{Re}}\right) \tag{9}$$

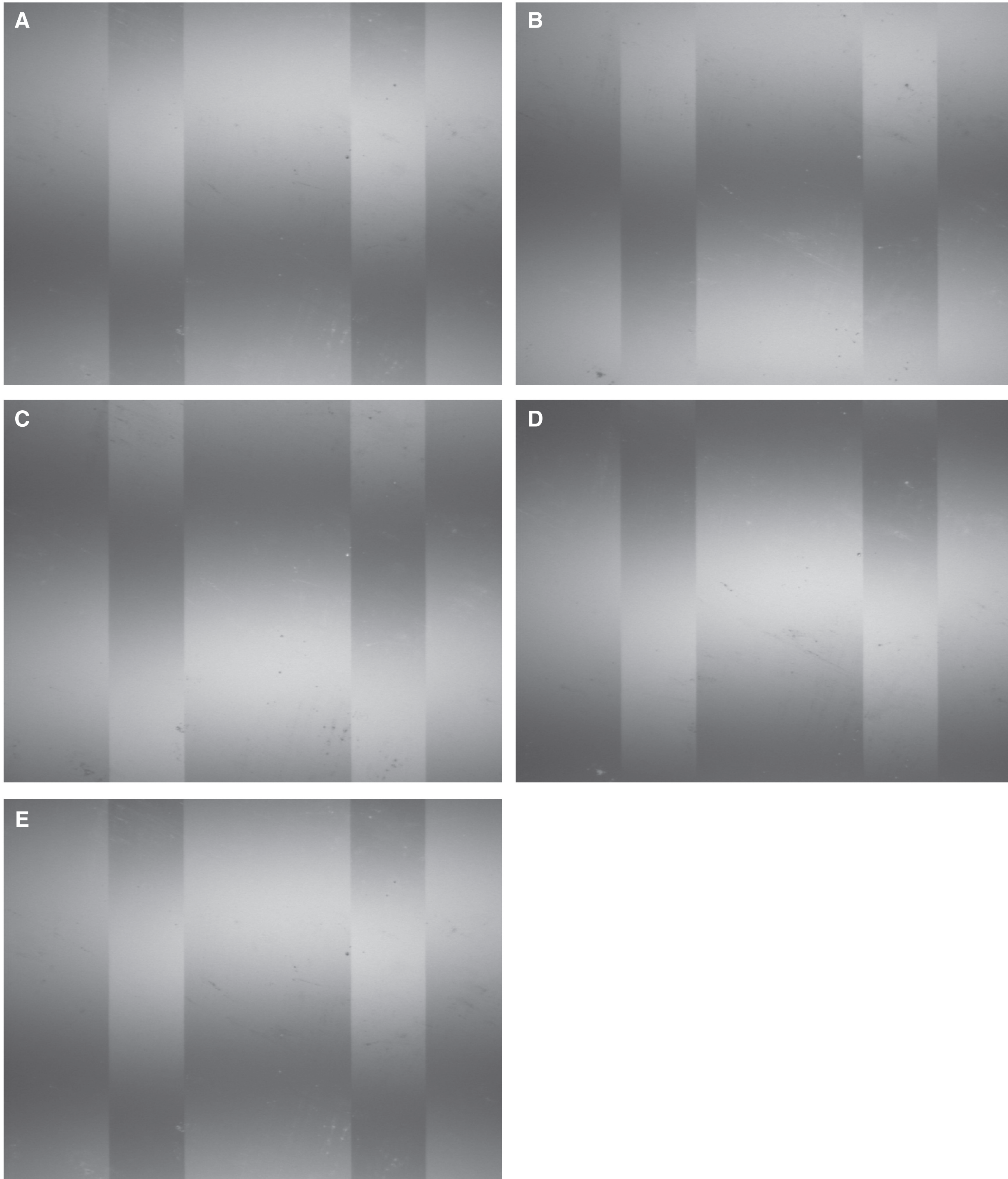

Figure 3 Interferogram for phase shifts in the following five steps: (A) 0°; (B) 90°; (C) 180°; (D) 270°; and, (E) 360°.

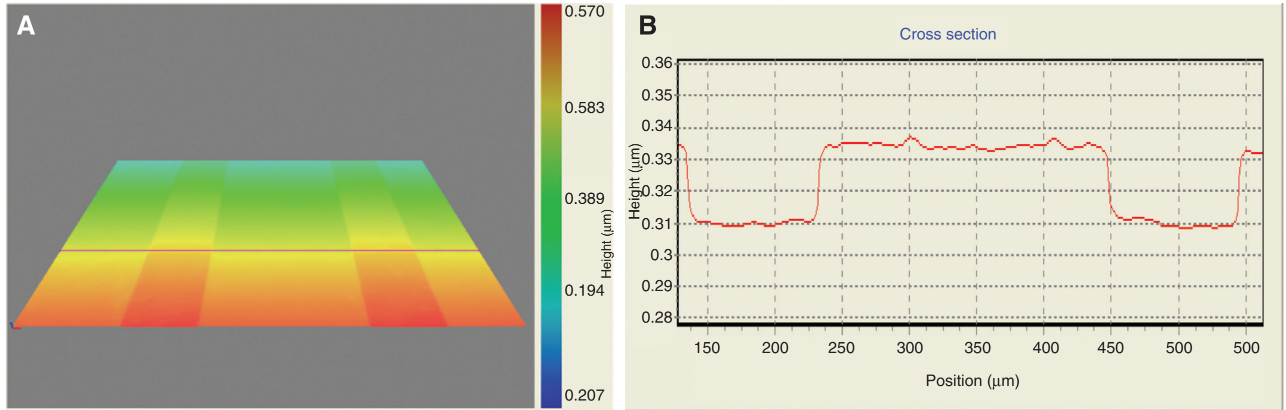

Figure 4 Measurement of a standard step height: (A) 3D profile of a standard step height and (B) the cross section of the measured sample.

The Euler equation considers the signs of both real and imaginary components and places the angle in the correct quadrant [18]:

$$\phi(x,y)=\begin{cases}\phi(x,y) \text{ for Im}\geq 0 \text{ and Re}>0\\ \phi(x,y)+\pi \text{ for Re}<0\\ \phi(x,y)+2\pi \text{ for Im}<0 \text{ and Re}<0\\ \frac{\pi}{2} \text{ for Im}>0 \text{ and Re}=0\\ \frac{3\pi}{2} \text{ for Im}<0 \text{ and Re}=0\end{cases} \tag{10}$$

Figure 3 shows an example of measurement results for a standard step height. Figure 3A shows the 3-D profile of the measured object, and Figure 3B shows a 2-D cross section of the profile. The nominal value of the step height is 24 nm (written as 0.024 µm on the sample) and the measured result for 30-time measurement is 24.2±0.058 nm. A Mirau interferometric objective with 20× magnification was employed in this measurement. Figure 4(A) and (B) illustrate the 3-D map of the reconstruction and the cross section along the red line marked on Figure 4(A), respectively.

The principle of using the developed SCSI system for dynamic surface profile measurement was comprehensively described in [12, 19, 20]. The CSI is used to reconstruct the surface profile of the vibrating object. In this study, an AFM cantilever was used to perform this test. The sample was vibrated at its first resonant frequency. The previous measurement in this system was 81.018 kHz. Figure 5A–D show 2-D cross section profiles of the AFM cantilever beam.

2.2 Resonant frequency detection for out-of-plane vibration

Resonant frequency in a mechanical system is the frequency that induces vibration to a maximum amplitude. In the white light interferometric system, this phenomenon is clearly observable and is automatically detected by the change in the interferogram pitch during vibration. The amplitude of the vibration changes the pitch of the interferogram fringes, and the interferometric fringe pitch decreases

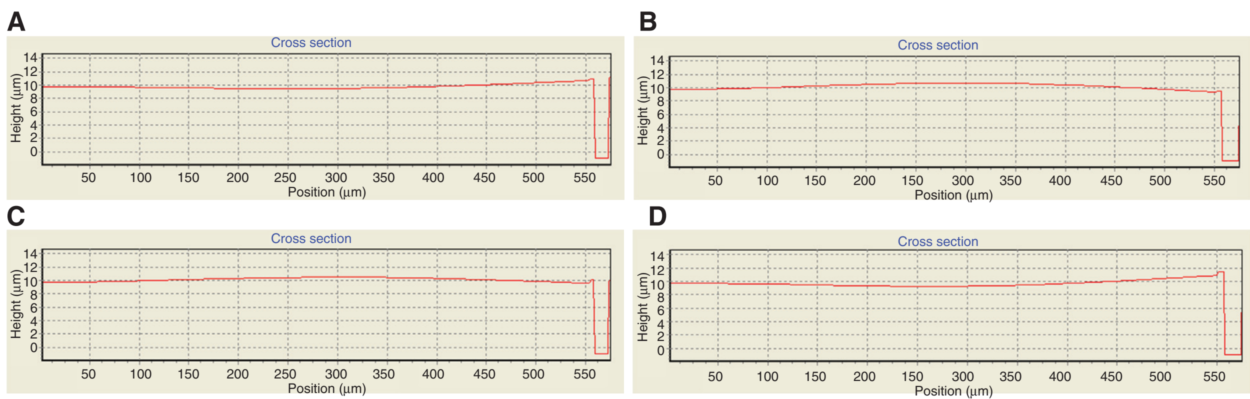

Figure 5 SCSI measurement results for AFM cantilever beam vibrating at 81.018 kHz at phase delay: (A) 0°; (B) 90°; (C) 180°; and, (D) 0°, respectively; and the 2D cross section at phase delay: (A) 0°; (B) 90°; (C) 180°; and, (D) 270°, respectively.

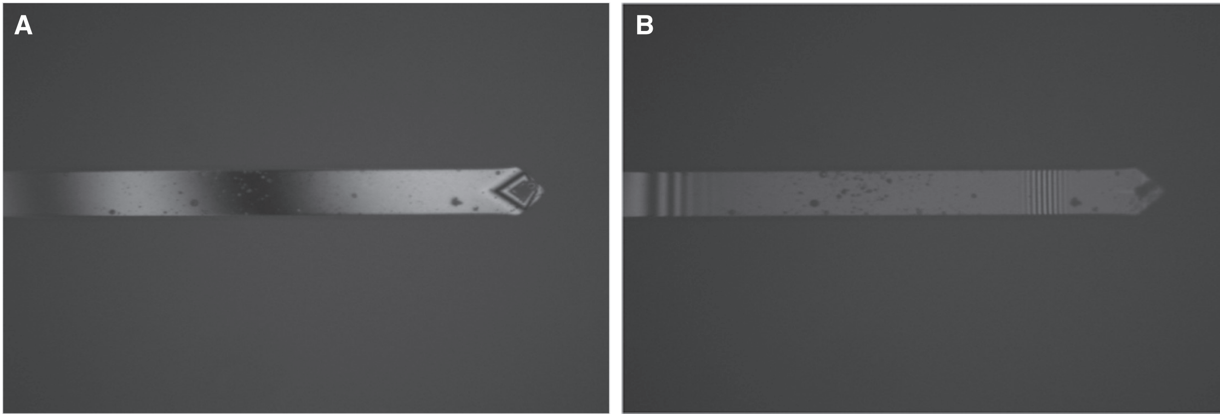

Figure 6 Interferogram of the AFM cantilever vibrating at (A) non-resonant frequency and (B) resonant frequency.

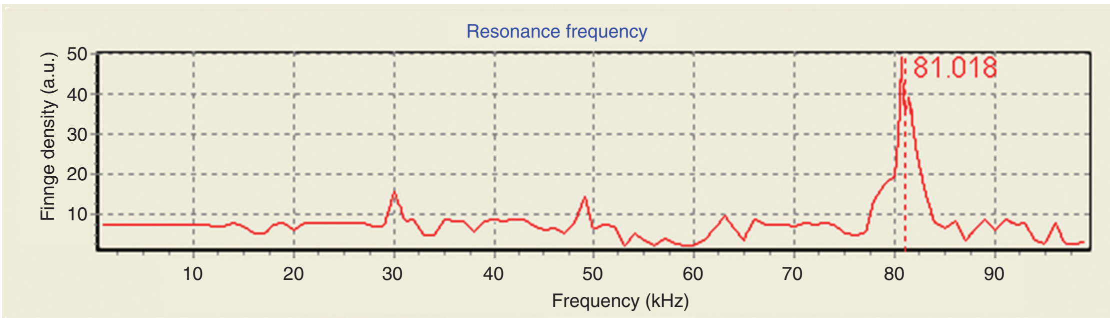

Figure 7 Results for out-of-plane resonant frequency measurement of the AFM cantilever beam.

as the vibration amplitude increases. This effect was demonstrated by an experiment in an AFM cantilever beam.

Figure 6A shows the interferogram of the sample when the vibration frequency is not the resonant frequency. In contrast, Figure 6B shows the interferogram of the sample when vibrated at its resonant frequency. The Figures show that the pitch of the interferometric fringe is reduced to a minimal value when the sample is vibrating at its resonant frequency. This behavior enables accurate scanning and detection of the resonant frequency by recording and detecting the pitch of the interferometric fringe during the sample out-of-plane vibration.

Based on the above principle, the resonant frequency is detectable by analyzing the spatial frequency of the interferogram at different scanning frequencies of the sample. The most effective method for analyzing the spatial frequency component of the interferogram is Fast Fourier Transform (FFT), which accurately extracts the frequency components and spectrum analysis.

The frequency scanning procedure is performed in a coarse scanning stage and in a fine scanning stage. With the coarse scanning result obtained (f_{coarse}), the fine scanning is then performed around f_{coarse} with an adequate frequency scanning pitch when the scanning range is set from (f_{coarse}-1) to (f_{coarse}+1) kHz with a frequency scanning pitch of 0.1 kHz. In this range, the same spectrum analysis

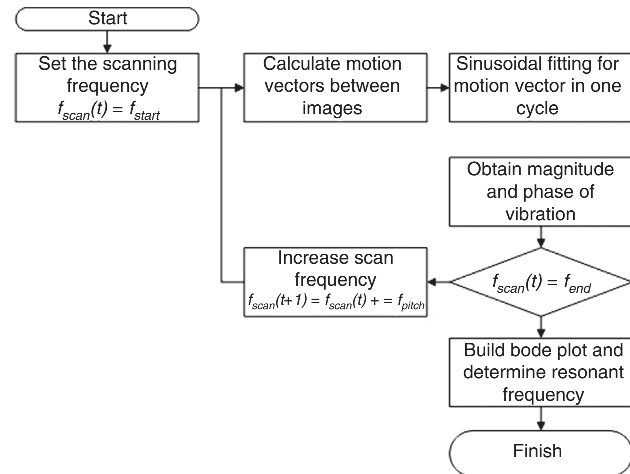

Figure 8 Flowchart of in-plane resonant frequency measurement process.

algorithm is used for the final frequency scan, and centroid detection method is used to calculate the fine peak. Figure 7 shows the density of the fringe as a function of frequency. As seen in Figure 7, a resonant frequency of 81 kHz was detected by the coarse scan and 81.018 kHz then detected from the fine scan. The repeated measurement had a standard deviation of 0.12 kHz. The resolution of resonant frequency detection can be increased by using a finer frequency scanning pitch.

According to the deconvolution algorithm developed in Ref. [12], the seventh-mode resonant frequency of the cantilever beam in the tested AFM was 3.7334 MHz, which was consistent with the theoretical estimation. This indicates that the measurement bandwidth of the developed testing platform can reach several megahertz.

2.3 Resonant frequency detection for in-plane vibration

The developed system can use a similar scanning frequency detection principle to detect in-plane resonant frequency through the developed in-plane resonant frequency scanning process described in Figure 8. A region of interest (ROI) is first set at the vibrating region of the device. The change in motion is then tracked by capturing a series of images at different phases of vibration. The algorithm searches the resonant frequency in the wide range $[f_{start}, f_{end}]$ with the resolution of f_{pitch} in the searching step. At each scanning frequency, motion vectors between images that have different vibration phases are identified, and a motion vector table is created to analyze the magnitude of difference in one cycle of vibration. The motion vectors are converted to actual displacement after using a standard resolution target (USAF 1951) to calibrate the lateral resolution of the microscope. The lateral resolution of the developed system using 50× microscope objective is 0.140 µm/pixel.

The above detection process uses a sub-pixel template matching technique based on image correlation to increase accuracy in measuring motion vectors. The template must be matched at every possible orientation of the sample. A matching score based on normalized cross correlation is evaluated at each orientation and the highest matching score determines the motion vector. The formula of normalized cross correlation is calculated for each orientation, and the highest matching score determines the motion vector. The formula for the normalized cross correlation is

$$c=\frac{n\sum_{i,j}A_{ij}B_{ij}-\sum_{i,j}A_{ij}\sum_{i,j}B_{ij}}{\sqrt{n\left(\sum_{i,j}A_{ij}^{2}\right)-\left(\sum_{i,j}A_{ij}\right)^{2}}\sqrt{n\left(\sum_{i,j}B_{ij}^{2}\right)-\left(\sum_{i,j}B_{ij}\right)^{2}}} \quad (11)$$

where c is cross correlation; n is the number of pixels in the template or source image; A_{ij}, B_{ij} are intensities of the template and source image at position (i, j) of image coordinate, respectively.

When objects in the image are rotated with respect to each other, a set of templates at different orientations is employed for matching. The rotation invariant template matching method employs the fluctuating scope of the

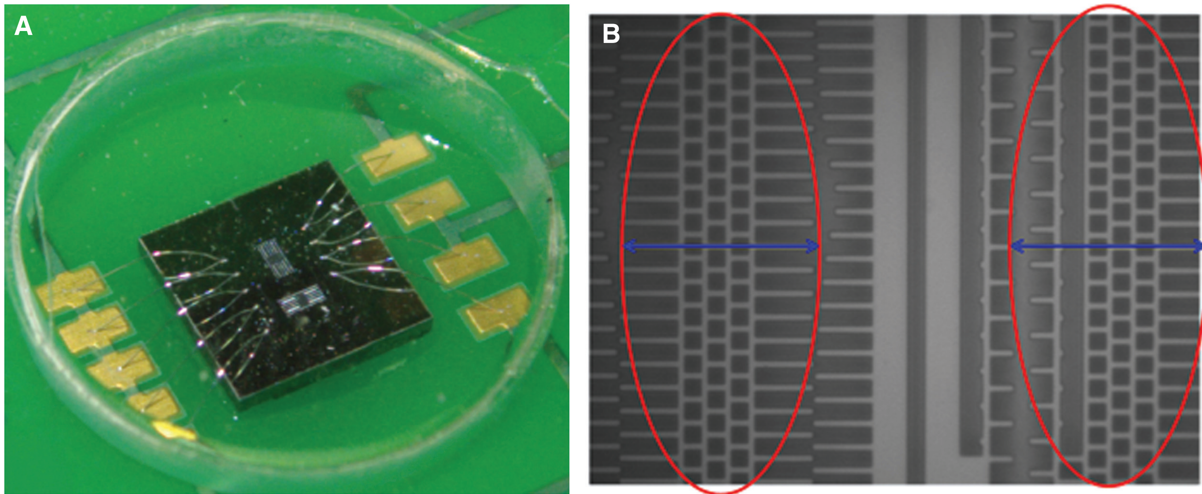

Figure 9 In-plane measurement of a MEMS comb drive: (A) Image of a MEMS comb drive and (B) vibrating parts of the comb drive captured by the microscopic system.

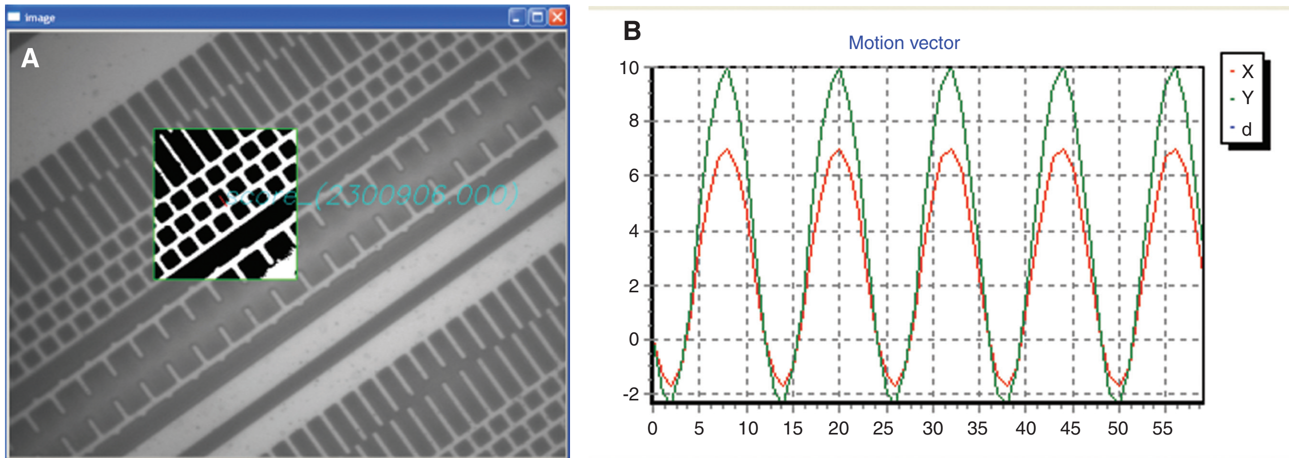

Figure 10 Measurement result of a motion vector: (A) the region of the comb drive used for motion vector calculation; and (B) the calculated motion vector.

rotation angle which can be adequately defined in the template image. The search process compares all template patterns with a source image.

Notably, two methods can be used to improve the acquired image quality in the developed system. One is to increase the spatial resolution of the hardware setup. The other option is to resample the image intensity to a higher spatial resolution through sub-pixel interpolation. Since the intensity interpolation approach is generally independent of image resolution, this method was applied in this study. The resolution of the original image can be increased by multiplying the image dimensions and their intensity values. After the multiplication process, a median filter is used to smooth the image while maintaining the continuity of image intensity. The motion vectors are calculated by conventional template matching for new images. The actual motion vectors of the original image can be obtained by dividing the motion vectors of the new images to the multiplied coefficient.

The tested sample is an electrostatic comb drive with an actuator that enables comb structures to be moved simultaneously by applying a voltage and an excited frequency. In the measurement experiment, the resonant frequency of the comb drive and applied voltage were 2.7 KHz and 5 V, respectively. Figure 9A, B illustrate the image of the comb drive and its captured images from the developed SCSI system, respectively. Figure 9B shows that the center of the drive is stationary. The two moving structures in the drive are indicated by the red ellipses.

Figure 10 shows the motion vector obtained by the developed cross correlation method, and Figure 10A shows the region of the MEMS where the motion vectors are detected. Figure 10B displays the resulting motion vectors.

Generally, a Bode plot can describe the characteristics of the vibration. A Bode plot includes a magnitude plot, which expresses the magnitude of the frequency response gain and phase plot, which expresses the frequency response phase shift. Figure 11 shows that a Bode plot is established by using a sinusoidal fitting technique to express the detected motion vectors as the magnitude and phase shift at each frequency.

After the Bode diagram is completed, the resonant frequency of in-plane motion can be further detected by finding the peak position in its magnitude diagram. In Figure 12, the magnitude versus frequency diagram clearly indicates the effect with the highest and sharpest peak, which is represented by the region where the resonant frequency occurs. The scan was performed at a range of 0.1–5 kHz and at a pitch of 0.05 kHz. The resonant frequency of the tested sample shown in Figure 9A was measured as 2.700 KHz. The repeated measurement result of resonant frequency is 2.692±0.012 kHz.

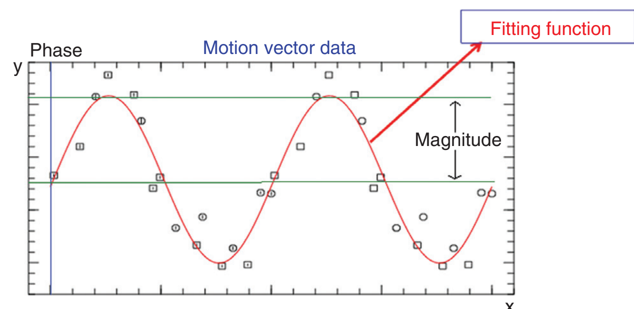

Figure 11 Sinusoidal fitting for calculating vibration magnitude and phase.

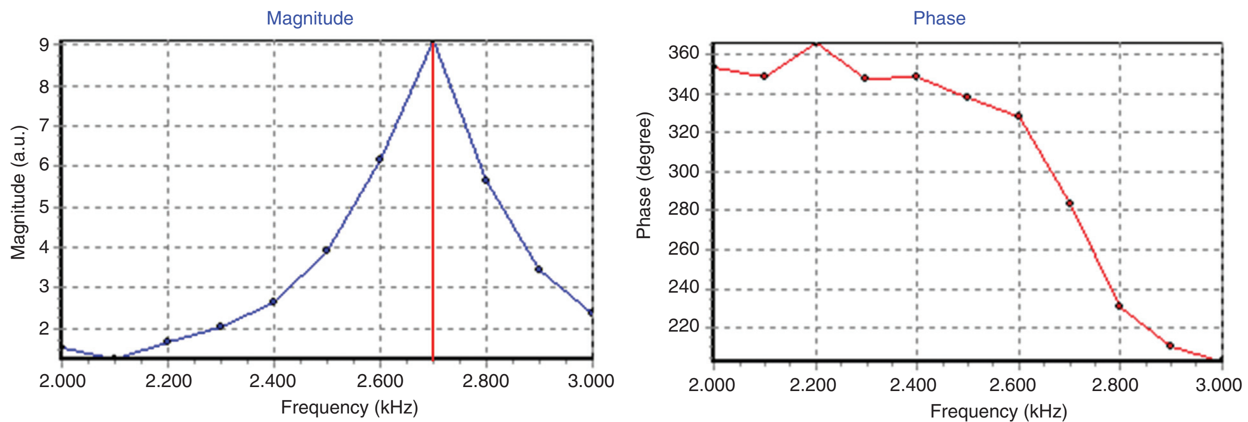

Figure 12 Resonant frequency determination from magnitude and phase plot.

3 Conclusions

A multi-function optical inspection methodology using SCSI was developed for identifying key characteristics of MEMS by both in-plane and out-of-plane measurement. Experiments showed that the developed methods are effective for 3D profile measurement in both static and dynamic samples. Meanwhile, a series of the resonant frequencies of the tested object can be precisely characterized for both of in-plane and out-of-plane vibration. The developed detecting principle and process enables accurate measurement of resonant frequency. The out-of-plane vibrating mode can be reconstructed by CSI with a vertical accuracy up to 10 nm and a detecting frequency can reach to several megahertz. The accuracy of the developed system was validated using standard samples. Full-field and high S/N measurement of CSI can be fully embedded with the developed method for profilometric characterization of MEMS in both static and dynamic modes. For these reasons, the SCSI method is superior to laser detection strategies.

References

[1] G. Coppola, P. Ferraro, M. Iodice, S. De Nicola, A. Finizio, et al., in ‘Microelectronics, 2004. 24th International Conference on, 2004’, pp. 213–216 vol.211.
[2] L. T. Wang, C. E. Stroud and N. A. Touba, ‘System-On-Chip Test Architectures: Nanometer Design for Testability’, (Elsevier Science Limited, 2008) pp. 591–651.
[3] K. Speller, H. Goldberg, J. Gannon and E. M. Lawrence, Proc. SPIE 4827, 478–485 478 (2002).
[4] A. Bosseboeuf, J. P. Gilles, K. Danaie, R. Yahiaoui, M. Dupeux, et al., Proc. SPIE 3825, 123–133 (1999).
[5] S. Petitgrand, R. Yahiaoui, K. Danaie, A. Bosseboeuf and J. P. Gilles, Opt. Laser. Eng. 36, 77–101 (2001).
[6] C. Rembe, R. Kant and R. S. Muller, Proc. SPIE 4400, 127–137 (2001).
[7] G. Coppola, P. Ferraro, M. Iodice, S. De Nicola, A. Finizio, et al., Meas. Sci. Technol. 15, 529–539 (2004).
[8] A. Bosseboeuf and S. Petitgrand, J. Micromech. Microeng. 13, S23–S33 (2003).
[9] K. Nakano, H. Yoshida, K. Hane, Trans. SICE 31, 454–460 (1995).
[10] P. de Groot, Appl. Opt. 45, 5840–5844 (2006).
[11] S. Petitgrand and A. Bosseboeuf, Proc. SPIE 5145, 33–44 (2003).
[12] L.-C. Chen, Y.-T. Huang, X.-L. Nguyen, J.-L. Chen and C.-C. Chang, Opt. Laser. Eng. 47, 237–251 (2009).
[13] P. Montgomery, F. Anstotz and J. Montagna, Proc. SPIE 8082, 808210–808210 (2011).
[14] J. Seppä, I. Kassamakov, V. Heikkinen, A. Nolvi, T. Paulin, et al., Opt. Eng. 52, 124104–124104 (2013).
[15] W. K. Chong, X. Li and S. Wijesoma, Opt. Lett. 35, 2946–2948 (2010).
[16] V. Heikkinen, I. Kassamakov, T. Paulin, A. Nolvi and E. Hæggström, Opt. Express 21, 5247–5254 (2013).
[17] B. Serio, J. J. Hunsinger and B. Cretin, Rev. Sci. Instrum. 75, 3335–3341 (2004).
[18] D. C. Ghiglia and M. D. Pritt, ‘Two-dimensional phase unwrapping theory, algorithms, and software’, Wiley, New York, 1998.
[19] L.-C. Chen, X.-L. Nguyen, H.-S. Huang and J.-L. Chen, Industrial Electronics, IEEE Transactions on 57, 1120–1126 (2010).
[20] L.-C. Chen, Y.-T. Huang, K.-C. Fan, IEEE-ASME Transations on Mechatronics, 12, 299–307 (2007).